Current Research in Food Science 5 (2022) 2219–2227

Contents lists available at ScienceDirect

Current Research in Food Science

journal homepage: www.sciencedirect.com/journal/current-research-in-food-science

Enzymatic acylation of cyanidin-3-*O*-glucoside in raspberry anthocyanins for intelligent packaging: Improvement of stability, lipophilicity and functional properties

Yang Lin [a,1], Cong Li [a,1], Ping Shao [a,b,*], Ligang Jiang [c], Bilian Chen [d], Mohamed A. Farag [e]

[a] Department of Food Science and Technology, Zhejiang University of Technology, Zhejiang, Hangzhou, 310014, PR China
[b] Eco-Industrial Innovation Institute ZJUT, Zhejiang, Quzhou, 324000, China
[c] Proya Cosmetics Co., Ltd, Zhejiang, Hangzhou, 310012, China
[d] Zhejiang Institute for Food and Drug Control, Hangzhou, 310052, China
[e] Pharmacognosy department, Faculty of Pharmacy, Cairo University, Cairo, 11562, Egypt

ARTICLE INFO

Keywords:
Enzymatic acylation
Raspberry anthocyanin
Cyanidin-3-*O*-Glucoside
Antioxidant activity
Stability
Intelligent food packing

ABSTRACT

Anthocyanins (ACNs) as one category of water-soluble flavonoid pigments are increasingly employed in pH sensing indicator applications for monitoring food freshness. Nevertheless, considering that anthocyanins are sensitive to environmental factors, their practical applications in food industries are still rather limited. In order to improve the stability of anthocyanins and capitalize upon their application in pH-color responsive intelligent packaging, this study aims to graft octanoic aid onto raspberry anthocyanins catalyzed by immobilized *Candida antarctica* lipase B (Novozymes 435). Structural analyses based on Fourier transform infrared spectroscopy (FTIR), UV–Vis, liquid chromatography-mass spectrometry (LC-MS), and nuclear magnetic resonance (NMR) revealed that octanoic acid was regioselective grafted onto the 6-OH position of its glucoside. The acylation efficiency of C3G by octanoic acid up to 47.1%. The octanoic acid moiety was found to improve lipophilicity, antioxidant activity and stability of C3G. In addition, acylated derivative also maintained the pH-color response characteristics of nature ACNs and exhibited excellent NH_3 response properties. These results indicated that acylated anthocyanins exhibit potential application as intelligent packaging indicator for monitoring food freshness.

1. Introduction

With a growing interest in healthy lifestyle, the consumer demand for high-quality food is on the rise (Becerril et al., 2021). Among the various attributes of food, freshness is one of the primary food attributes that consumers consider first acting as a reliable indicator to guarantee the safety and quality of packaged food (Oladzadabbasabadi et al., 2022). Food packaging is one of the important physical barriers to prevent food from microbial contamination, damage and loss (Cheng et al., 2022). Since fermentation or spoilage degree of packaged food products is generally associated with pH changes, the concept for pH response intelligent packaging has been developed in recent years (Shao et al., 2021). This type of intelligent packaging can monitor or sense the current conditions of packaged food as well as the environmental changes to occur inside the package using color changes of pH sensitive dyes, thereby informing consumers of products' status in real time (Rawdkuen et al., 2020).

According to previous studies, chemical dye indicators, such as neutral red, methyl orange, bromocresol green, bromothymol blue, and bromocresol purple have been used as pH indicator packaging materials (Oladzadabbasabadi et al., 2022). However, there are a number of issues related to chemical dye indicators including their safety and possible migration in food-packaging (Fei et al., 2021). Therefore, non-toxic naturally occurring pH indicators especially anthocyanin-rich extracts obtained from plants are regarded as best alternative (Rawdkuen et al., 2020).

Anthocyanins (ACNs) widely distributed in fruits and vegetables such as sweet potatoes, red cabbage, cranberry, and raspberry (Cai et al., 2020; Neves et al., 2022). A large number of studies demonstrated that ACNs from natural sources possess a wide spectrum of potential

* Corresponding author. Department of Food Science and Technology, Zhejiang University of Technology, Zhejiang, Hangzhou, 310014, PR China.
E-mail address: pingshao325@zjut.edu.cn (P. Shao).
[1] Yang Lin and Cong Li, contributed equally.

https://doi.org/10.1016/j.crfs.2022.11.008
Received 11 September 2022; Received in revised form 24 October 2022; Accepted 3 November 2022
Available online 5 November 2022

functional properties, including anti-oxidant, anti-inflammation, anti-aging, anti-cancer, and neuro-protection (Sreerekha et al., 2021). In addition, ACNs change from red flavylium to purple/blue quinoidal base, colorless hemiketal, or yellow chalcone upon pH changing from acidic to alkaline (Rawdkuen et al., 2020). In view of their broad-spectrum safety, antioxidant activity and pH responsive characteristics (Filho et al., 2021; Qin et al., 2021), several intelligent food packaging films based on natural ACNs have been fabricated to monitor food freshness or likewise spoilage (Filho et al., 2021; Qin et al., 2021). However, due to the presence of the flavylium ion and its peculiar electron distribution, ACNs are sensitive to environmental factors such as pH, storage temperature, light, oxygen, enzymes, and metallic ions (Tarone et al., 2020). Natural ACNs are relatively unstable thereby interfering with our perception of food freshness and restricting their effectiveness in smart food packaging (Almasi et al., 2022; Yong and Liu, 2020). Previous studies revealed a correlation between the stability and ACNs structure with increase of hydroxyl groups found to reduce its stability, whereas increase of methoxy groups showed opposite effect (Becerril et al., 2021). In recent years, anthocyanins glycosyl acylation has become a promising tool to enhance ACNs stability during food processing and storage (Zhao et al., 2021). Generally, acyl donor can be linked and packed onto the core structure of ACNs to hide active sites by acylation, thereby effectively preventing attacks from hydrophilic groups and deactivation caused by other factors (Zhao et al., 2017). Up till now, most studies on acylation in ACNs have focused on enhanced stability and antioxidant activity (Cai et al., 2020; Liu et al., 2020; Yang et al., 2019). Correlation analysis between enhanced stability of acylated derivatives and its intelligent indication effect has not yet been established. The sensitivity and persistence of acylated derivatives for monitoring food freshness remain to be assessed.

In this study, the main ACN (cyanidin-3-*O*-glucoside) from raspberries was successfully extracted and purified. Octanoic acid was grafted onto raspberry ACNs using enzymatic acylation, and the structure of acylated ACNs was characterized by LC-MS and NMR. The application prospect of fatty acid acylated ACNs intelligent indicator packaging was investigated through analyzing correlation between stability, antioxidant properties and intelligent packaging efficiency. Our research provides a potential improvement for the application of ACNs in intelligent food packaging.

2. Experiment

2.1. Materials and reagents

Raspberry powder was purchased from Nanjing Plant Origin Biological Co., Ltd. (Nanjing, China). Lipase (Novozymes 435, ≥9000 PLU/g) was obtained from Beijing Gao Ruisen Technology Co. Ltd. 4 A molecular sieves and β-carotene were purchased from Aladdin Chemistry Co., Ltd. (Shanghai, China). Octanoic acid was purchased from Shanghai Titan Science and Technology Co., Ltd. (Shanghai, China). Tert-butyl alcohol, ethyl acetate, tween 80, linoleic acid, n-octanol were supplied by Rhawn Biotechnology Co., Ltd. (Hangzhou, China). *N, N*-Dimethylformamide (with molecular sieves, Water ≤50 ppm) (DMF) was purchased from J&K Scientific Co., Ltd. (Beijing, China). 2,2-Diphenyl-1-picrylhydrazyl (DPPH >99%) was provided by Yuanye Bio-Technology Co., Ltd. Ultrapure water (Milli-Q) was used to prepare all solutions.

2.2. Extraction and purification of anthocyanins from raspberry

The fresh raspberries were freeze-dried into powder then dissolved in 90% ethanol solution at a ratio of 1:15, and flash extractor with 150 voltage and extraction time of 75 s were employed, according to Teng et al. (2021). The supernatant was filtered, and subjected to lyophilization till complete dryness and stored away from light at −20 °C. Afterwards, anthocyanins were purified using NKA-9 microporous resin, eluted successively with distilled water, ethanol and methanol, according to Meng et al. (2018). Finally, anthocyanins in the collected eluent were analyzed using HPLC according to Teng et al. (2021).

2.3. Preparation of enzymatic acylated ACNs and product isolation

Enzymatic acylation of purified ACNs was performed in an Erlenmeyer flask, according to a previously reported method with slight modifications (Yang et al., 2018). Purified ACNs (98%, 1 mg/mL) was dissolved in tertiary butanol and DMF was then added to this solution as a cosolvent (at a volume ratio of tert-Butanol/DMF of 9:1). After overnight drying with freshly activated molecular sieves (4 Å), tertiary butanol was mixed with octanoic acid at a molar ratio of ACNs/acyl donor of 1:10 M. The Novozymes 435 was added to the reaction mixture at 20 g/L. Enzymatic acylation was proceeded for 24 h at 60 °C with stirring at 350 rpm. The enzyme was removed to terminate reaction by filtration using a membrane filter (50 mm inner diameter, 0.22 μm, Meryer Chemical Technology Co., Ltd. Shanghai, China).

Extraction and separation of acylated derivative were performed following the method described by Li et al. (2022), with slight modifications. The reaction mixture was transferred to a separatory funnel, successively extracted with saturated sodium chloride (50 mL), sodium bicarbonate (50 mL) and ethyl acetate (100 mL), sufficient oscillation and then left to stand until complete separation. The upper ethyl acetate phase was collected and the lower aqueous phase continued to be extracted with ethyl acetate. Extraction was repeated until ethyl acetate phase was transparent. The ethyl acetate phase was combined and solvent evaporated under reduced pressure at room temperature. Finally, acylated ACNs with octanoic acid was collected after freeze-drying.

2.4. HPLC-DAD-MS/MS analysis

Chromatographic separation was performed on an Agilent 1100 high performance liquid chromatography (HPLC) system, equipped with a diode array detector (Agilent 1100) and a welch ultimate XB-C18 (2.1*100 mm, 3 μm). Samples were dissolved in HPLC grade 100% methanol (2 mg/mL) and passed through a 0.22 μm membrane filter. The detection was performed at 520 nm. Acylated ACNs were eluted using 0.1% formic acid/water as solvent A and acetonitrile as solvent B. The gradient program of the mobile phase was as follows: 0–10% B over 8 min, 10–94% B over 11.5 min, and 94% B elute for 15 min at a flow rate of 0.3 mL/min. The sample injection volume and column temperature were set at 4 μL and 30 °C, respectively. The acylation efficiency was calculated based on peak area reduction of C3G before and after acylation (Zhang et al., 2021).

Mass spectroscopy (MS) analysis was performed using a Thermos TSQ Quantum Ultra (Thermo Fisher Scientific, USA) with an electrospray ionization (ESI) interface, further determining ion products structure. The ESI source was set in positive ionization mode considering anthocyanins improved detection in that mode. The capillary temperature was set at 350 °C. The spray voltage was 3.3 kV, heater temperature was 450 °C and the tube lens off was set to −19 V. The sheath gas pressure and the aux gas pressure were set at 42 and 13 Arb, respectively. Mass spectra were acquired by scanning ions ranging from m/z 50 and 1200. The ion Sweep Gas Pressure and the source collision-induced dissociation (CID) were set at 1 and 0 V, respectively.

2.5. Purification of acylated derivatives with semi-preparative HPLC

The acylated ACNs were isolated using an LC3000 semi-preparative HPLC system, with a P3000 high pressure pump, Rheodyne manual injection valve model 7125 and an UV 3000 ultraviolet–visible (UV–vis) detector (Innovation Tong Heng Technology Co., LTD, Shanghai, China) at room temperature 25 °C. A Phenomenex Aeris PEPTIDE XB-C18 column (10 μm, 250 × 20 mm) was employed for the isolation of acylated derivatives. Methanol was used to dissolve acylated derivatives.

Acetonitrile and 0.1% formic acid water were used as solvent A and B with gradient elution at a flow rate of 20 mL/min. The gradient program of the mobile phase was as follows: 0–5 min, 0–70% B; 5–15 min, 70−10% B and 15–20 min, 10% B. The injection volume was set at 200 μL, and the column temperature was maintained at 25 °C. The collected fractions of acylated ACNs were evaporated at room temperature 25 °C to remove organic solvents, freeze-dried, and stored at −80 °C prior to NMR analysis.

2.6. Characterization of ACNs and its acylated derivative

Fourier transform infrared spectra were recorded on a Nicolet iS 50 FT-IR Spectrometer (Thermo Scientific) to identify functional groups in ACNs and acylated ACNs with the wave number region ranging from 4000 cm^{-1}–500 cm^{-1} at a resolution of 16 cm^{-1}. The UV–vis absorbance spectra were recorded by M9 xenon lamp spectrophotometer (Shanghai Mapada Instruments Co. Ltd., China) to compare the differences between ACNs and its acylated derivative. The structure of purified sample (5 mg) was analyzed by Bruker AVANCE III 600 MHz NMR spectrometer (Shanghai, China). ^{1}H NMR and ^{13}C NMR spectra were recorded in dimethyl sulfoxide (DMSO) (500 μL) with tetramethyl silane (TMS) as an internal standard (chemical shifts (δ) in parts per million, coupling constants (J) in hertz). ^{1}H chemical shifts were assigned using 2D NMR (COSY) experiment, while ^{13}C resonances were assigned using 2D NMR experiments (gHMBC and gHSQC).

2.7. Determination of lipophilicity and antioxidant activity

2.7.1. Lipophilicity

The lipophilicity of acylated ACNs was determined using octanol/water partition coefficient (log P). Briefly, n-octanol was pre-saturated with acidified water (2% HCl) (3:1, v/v) for more than 24 h. The absorbance (A_0) of ACNs and its acylated derivative dissolved in saturated 1-octanol was determined at 520 nm. Later, the same volume of acidified water (2% HCl) saturated with n-octanol was added. The mixture was fully oscillated for a period of 1 h, and centrifuged at 2000 g for 10 min. The absorbance (Ax) of the upper 1-octanol solution was measured at 520 nm as described by Yang et al. (2018). The syringe used to collect the water-rich phase was filled with air, which was inserted slowly while passing through the octanol phase. The octanol/water partition coefficient (log P) was calculated using the following equation (1):

$$log\ P = log\ [A_x / (A_0 - A_x)] \quad (1)$$

2.7.2. DPPH free radical scavenging activity assay

The DPPH free radical scavenging activity assay was performed according to the method of Lin et al. (2020), with minor modifications. ACNs and acylated ACNs were prepared in mother liquor at a concentration of 250 mg/L anthocyanidin equivalent. 100 μL Blank (PBS) and sample were plated two times in two 96-well plates. Then, 100 μL DPPH• solution (10 μM) and methanol were separately added to plate 1 and plate 2. The plate was wrapped with an aluminum foil and incubated in the dark for 30 min. The absorbance was measured at 517 nm, and percentage of DPPH inhibition was calculated using equation (2) as follows:

$$DPPH\ Clearance\ (\%) = [(A_0 - A_1) / A_0] \times 100 \quad (2)$$

Where A_1 is the reading of methanol plate, A_0 is the reading of DPPH solution plate.

2.7.3. β-Carotene bleaching assay

The β-carotene bleaching assay was slightly modified from protocol described by Liu et al. (2020). Briefly, 10 mL of β-carotene in chloroform (1 mg/mL), 400 μL of linoleic acid and 4 mL of Tween 80 were thoroughly mixed in a 250 mL pear shaped bottle. After removing chloroform by rotary evaporator at 40 °C, 100 mL distilled water was added to the pear-shaped bottle and vigorously shaken to form emulsion. Thereafter, 10 mL of the emulsion was collected, and distilled water was added to a final volume of 100 mL to prepare the emulsion diluent. ACNs and acylated ACNs were prepared in mother liquor (1 mg/mL anthocyanidin concentration) using 30% ethanol. The anthocyanin solution (0.2 mL) was added to 4.8 mL of the emulsified diluent, and the corresponding absorbance (A_0^S) at 470 nm was determined after mixing. The sample was placed in a water bath at 50 °C for 2 h, and the absorbance value (A_2^S) at 470 nm was determined. Control sample was prepared using same conditions without anthocyanin solution being replaced with 70% ethanol solution. The inhibition capacity was calculated using the following equation (3):

$$\text{Inhibition rate}\ (\%) = [1 - (A_0^S - A_0^C) / (A_2^S - A_2^C)] \times 100 \quad (3)$$

Where A_0^S and A_2^S denotes for the absorbance value of the ACNs and acylated ACNs before and after heat treatment, respectively. A_0^C and A_2^C denotes the absorbance value of control sample before and after heat treatment, respectively.

2.8. Thermostability and photostability

A previously described method with slight modification was used to evaluate the thermostability and photostability of ACNs and acylated ACNs (Yang et al., 2018). ACNs and its acylated derivative were diluted to the proper concentration with a buffer solution (0.1 mol/L citric acid/sodium citrate, pH = 3.0), at which the absorbance at concentration maximum absorption wavelength ranged from 0.8 to 1.

The thermostability of ACNs and acylated ACNs were determined by incubation of ACNs and acylated ACNs solutions at 65, 80, and 90 °C, respectively, using a water bath and monitoring the change of anthocyanins concentration using the pH-differential method over time (Taghavi et al., 2022). To evaluate light stability, solutions of anthocyanin (20 mL) in screw-cap glass vial were placed under the incandescent light bulb (40 w) and ultraviolet illumination (253.7 nm/185 nm, ≥ 214 uw/cm^2) (Jiangyin Instrument Co., Ltd., Jiangyin, China) at 20 °C, with change in anthocyanin concentration over time determined using pH differential method. The concentration of ACNs and acylated ACNs was measured using UV spectrophotometry. The first-order reaction rate constant (k) and half-life time ($t_{1/2}$) of ACNs and acylated ACNs were determined using the following equations (4) and (5):

$$ln\ (C / C_0) = -k \times t \quad (4)$$

$$t_{1/2} = -ln\ (1/2) \times k^{-1} \quad (5)$$

where C_0 is the initial content of ACNs and acylated ACNs, C is the content of ACNs and acylated ACNs at time (t), k is the rate constant (h^{-1}), $t_{1/2}$ is half-life time.

2.9. pH-response and NH_3-response of ACNs and its acylated derivatives

The response characteristics of C3G and acylated C3G were obtained by using a spectral scanning by dissolving samples in different pH buffers (from 1.0 to 12.0) and storing them at 4 °C in dark for 24 h. The ammonia gas response property was also obtained by recording the absorption spectrum of samples under ammonia atmosphere over time using Conway dishes (Fei et al., 2021).

2.10. Statistical analysis

All assays were conducted in triplicates. SPSS 22.0 (SPSS Inc., USA) software was used for statistical analysis of the data. The differences between the average values for each treatment was obtained using one-way analysis of variance (ANOVA), $p \leq 0.05$ was considered statistically

significant differences. Figures were created using Origin Pro 2021 (Origin Lab, USA).

3. Results and discussion

3.1. Structural elucidation of acylated ACNs products from enzymatic acylation

3.1.1. LC-MS analysis

Cyanin-3-*O*-glusoside (C3G) was confirmed as the primary anthocyanin in raspberry, and the purity of C3G for 98.3% was obtained after purification using semi-preparative HPLC. Afterwards, acylation reaction between C3G and octanoic acid was performed using enzymatic catalysis. C3G and the reaction mixture were submitted to HPLC analysis and monitored at 520 nm for reaction monitoring. Chromatographic analyses of C3G and its acylated derivative using LC-MS analysis are presented in Fig. 1C and D, respectively. A main peak 1 was detected at 1.5 min (Fig. 1C) exhibiting a molecular ion (*m/z*) [M + H] + consistent with that of C3G (448.98) and showing decrease after acylation. C3G conversion efficiency using enzymatic acylation with octanoic acid as acyl donor was at 47.1% as evident by relative peak area measurement of a new peak 2, which appeared at 0.5 min after acylation. According to its full MS spectrum $[M + H]^+$ ion at *m/z* 575 (449 + 126) yielded fragment ion at *m/z* 287 from the parent ion *m/z* 575 in the MS^2 spectrum. The product was identified as a conjugate of C3G molecule with an extra octanoic acid moiety Cruz et al. (2017) and annotated as C3G-octanoic acid. This result indicated that enzymatic acylation reaction of C3G with octanoic acid was regioselective to the glycosidic moiety under the catalytic action of Novozymes 435. Enzymatic acylation preferentially occurred at a hydroxyl group in the sugar moiety instead of a hydroxyl group in cyaniding aglycone (Cruz et al., 2016). Additionally, Cruz et al. (2018) revealed that enzymatic acylated anthocyanin glucosides from blackcurrant (*Ribes nigrum* L.) skin extract was selective to cyanidin and delphinidin glycosides, but not the corresponding rutinosides.

3.1.2. UV–vis and FT-IR analysis

UV–vis absorption spectra for C3G and C3G-octanoic acid are depicted in Fig. 1A. The UV absorbance spectrum of C3G-octanoic acid was similar to that of C3G, indicating that acylation occurred not at the flavonoid moiety, but rather the sugar. The absorption at 278 nm and 510 nm of C3G were ascribed to the characteristic bands of anthocyanins, with the characteristic absorption peak at 510 nm showing hypochromic shift after acylation. Similarly, acylation using lauric acid as the acyl donor resulted in bathochromic shift that changes absorption maxima (λ max) from 517 nm to 525 nm (Yang et al., 2019). In our current study, acylation using octanoic acid as the acyl donor showed smaller bathochromic shift, with shift in (λ max) from 510 nm to 512 nm for C3G. A slight drop in absorbance was likewise observed at 510 nm after acylation. In detail, the increase of foreign groups (octanoic acid) in C3G, furthermore, part of the chromophore in C3G were destructed and/or degraded as manifested by decrease in absorbance (Cai et al., 2020; Liu et al., 2020). Results indicated that binding of fatty acid to ACNs resulted in shifting ACNs balance towards the colored flavylium cation form Zhao et al. (2021).

FT-IR study was further employed to assess the effect of acylation on C3G functional groups. Fig. 1B shows the FT-IR spectra of C3G and C3G-octanoic acid. The strong and broad absorption band of C3G at 3300 cm^{-1} was attributed to the stretching vibration of –OH, including the hydroxyl from aromatic ring and glycosyl in C3G octanoic acid (Cai et al., 2020). Compared with C3G, the peak of C3G-octanoic acid at 3343.53 cm^{-1} was significantly weaker due to acylation, which was in accordance with Xiao et al. (2021). The enhanced absorption bands at 2923.12 cm^{-1} and 2853.69 cm^{-1} in C3G-octanoic acid were attributed to $–CH_2$, $–CH_3$, and –CH stretching vibration in the glycosyl moiety (Liu et al., 2020). According to these spectral changes, octanoic acid was suggested to be included in the structure of ACNs. More importantly, FT-IR spectra of C3G showed a carbonyl (C═O) peak at 1740 cm^{-1} (Scano, 2021), which was shifted to 1730 cm^{-1} in the FT-IR spectra of C3G-octanoic acid likely due to conjugation of the aromatic ester carbonyl with C═C leading to C═O shift to a lower wavenumber. These changes indicated that octanoic acid was grafted onto the C3G molecule through acylation located at –OH of the sugar moiety in C3G and in accordance with UV results.

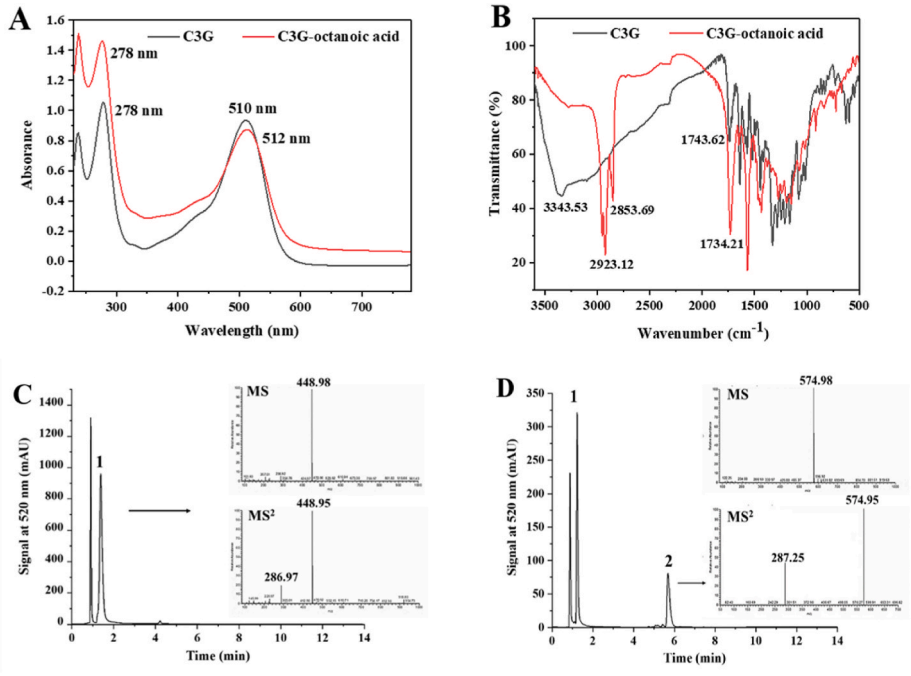

Fig. 1. Chemical structure analysis of raspberry anthocyanins and derivatives. UV–vis spectra of C3G and its derivative (A); FT-IR spectra of C3G and its derivative (B); LC-ESI-MS chromatograms showing C3G (C) and its derivative (D).

3.1.3. NMR analysis

To further clarify the structure of C3G octanoic acid and its acylation position, acylation product was subjected to NMR analysis post HPLC purification. The product was obtained as dark-purple amorphous powder with purity greater than 98% based on the comparison of peak areas at 280 nm. Chemical structure of the acylated product was determined using 1D and 2D NMR experiments dissolved in DMSO-d6/TFA 9:1 (Fig. 2). Compared with C3G, the chemical shifts of 6''a-H and 6''b-H of glucoside in C3G-octanoic acid were shifted downfield by ~0.2–0.5 Hz. The acylation took place at 6″–OH of glucose moieties according to the observed corresponding chemical shifts, which were similar to previous reports (Fernandez-Aulis et al., 2020; Yang et al., 2018).

3.2. Properties of acylated ACNs

3.2.1. Lipophilicity

In general, higher log P value indicates higher lipophilic property of the substance (Xiao et al., 2021). As shown in Fig. 3A, the partition coefficient (log P) of C3G as expectedly was significantly increased from −0.83 to 0.68 ($p < 0.05$) post acylation with octanoic acid. The log P of C3G-octanoic acid was much higher than that of C3G indicating that acylation of anthocyanins with fatty acid increases its lipophilic nature (Grajeda-Iglesias et al., 2017; Yang et al., 2018). Previous studies revealed that glycosyl groups attached to the C3 site are very active and can freely spin (Dangles et al., 1993), causing the acyl groups wrapping around the benzopyrylium ring (Zhao et al., 2017). The aliphatic acyl groups (octanoic acid) with comparatively high hydrophobic moiety wrapped around the structure of ACNs can effectively decrease their solubility in aqueous media thereby reducing hydration (Bailon et al., 2004). Steric hindrance created by octanoic acid prevents the possible ion from attacking anthocyanidins and stabilizes them further (Zhao et al., 2017). The enhanced lipophilic nature of acylated C3G significantly expands its application as colorants from aqueous to fat-rich food matrices such as oils and fats.

3.2.2. Antioxidant activity

As shown in Fig. 3B & C, antioxidant assays via DPPH and β-carotene bleaching assays showed higher antioxidant activity of C3G-octanoic acid than C3G. The DPPH clearance of C3G after acylation showed significant increase from 13.9% to 19.4% ($p < 0.05$). The enhanced antioxidant capacity of C3G-octanoic may be attributed due to its enhanced lipophilic nature after acylation (Plaza et al., 2014). Studies showed that lipophilicity affects flavonoids capacity to reach sites that are attacked by free radicals (Araújo et al., 2017). The aliphatic acyl groups (octanoic acid) with comparatively high hydrophobic moiety wrapped around the structure of ACNs can reduce hydration and C3G polarity, thereby leading to improved antioxidant activity (Bailon et al., 2004). The inhibition ratio in β-carotene bleaching assay of C3G was 37.4%, which was significantly increased to reach 71.05% ($p < 0.05$) post octanoic acid acylation, Fig. 3B. Further results of the β-carotene bleaching assay likewise showed improved inhibition of lipid peroxidation by acylation. It is more comparable to the actual lipid reaction environment due to the use of linoleic acid as the model lipid substrate (Yang et al., 2019). Meanwhile, steric hindrance created by octanoic acid prevents the possible ion from attacking anthocyanidins and to derive with antioxidant groups towards the oxidation interface of a lipid (Song et al., 2021).

Free radicals and other reactive oxygen species play a deleterious role in food systems, causing food spoilage and nutritional loss (Shao et al., 2021). Hence, antioxidant activity (the oxygen barrier ability of the films) is an important property for food packaging films to extend food shelf life (Mushtaq et al., 2018). The packaging films without ACNs (such as chitosan and starch films) usually exhibit lower antioxidant activity compared with those films blended with ACNs (Yong et al., 2020), while films with a high oxygen barrier ability can protect the packaged food from lipid peroxidation (Kurek et al., 2018). The addition of ACNs-rich extract can improve oxygen barrier ability of the film (Ge

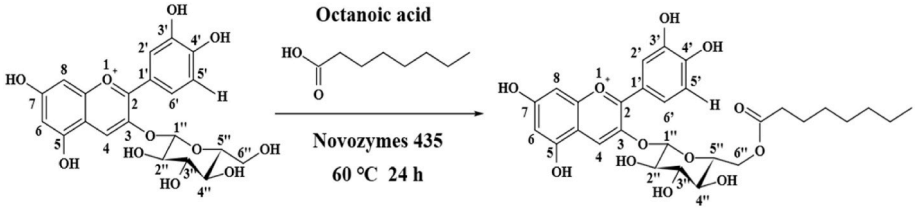

Position	C3G δ_H (ppm)	C3G-octanoic acid δ_H (ppm)
Anthocyanins		
4	8.88	8.78
6	6.88;	6.71
8	6.91;	6.89
2'	8.02	7.97
6'	8.17	8.21
5'	7.01	7.01
Glucose		
1''	5.29	5.41
2''	3.53	3.50
3''	3.37	3.39
4''	3.25	3.21
5''	3.71	3.78
6''a	3.82	4.34
6''b	3.85	4.05

Fig. 2. 1HNMR spectral data of C3G and its derivative. 1H and 13C NMR data of C3G-octanoic acid in DMSO-d6/TFA (9:1). Key: s, singlet; m, multiples; d, doublet; t, triplet; dd, double of doublets; * unresolved.

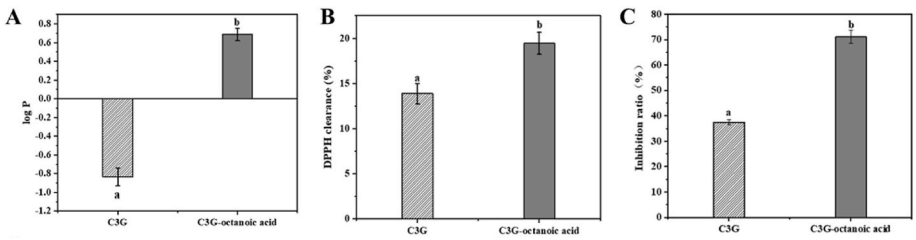

Fig. 3. Partition coefficient (log P) (A); DPPH radical scavenging capacity (B); β-carotene bleaching assay (C) of C3G and its derivative. Groups with different letters are significantly different from each other ($p < 0.05$).

et al., 2020). Therefore, acylated ACNs with enhanced antioxidant activity is expected to exhibit a wider application in intelligent food packaging.

3.2.3. Thermostability and photostability

The differences in thermal stability of C3G and C3G-octanoic acid after dissolving in aqueous hydrochloric acid (pH 3) was investigated. The logarithm of monomeric anthocyanin content (ln (C/C_0)) was plotted versus time (t) (Fig. S1), revealing that thermal degradation of C3G and C3G-octanoic acid followed first-order reaction kinetics with respect to temperature. The result was consistent with previous reports (Yang et al., 2018; Zhang et al., 2021). The kinetic parameters are summarized in Table 1. As expected, values of half-life ($t_{1/2}$) and reaction rate constant (k) showed that the thermostability of both C3G and C3G-octanoic acid decreased with increasing temperature (from 65 °C to 90 °C). The increase in environmental temperature conferred an active equilibrium shift of anthocyanins to shift towards colorless chalcone and pseudo base formation (Cai et al., 2022). The reaction rate constant (k) of octanoic acid conjugate at each selected temperature were all lower than those of C3G, while $t_{1/2}$ values were all higher than those of C3G. Acylation plays a significant role in the improvement of anthocyanin thermostability through "π−π" interactions between the acyl residues and anthocyanin nucleus to protect anthocyanin molecules from nucleophilic attack (Yan et al., 2016; Yang et al., 2018). Therefore, acylation prolonged the half-life of C3G thermal degradation, thereby exhibiting enhanced thermostability.

Table 1 presented the kinetic parameters for anthocyanins photodegradation under incandescent and UV light, indicating that acylation of C3G significantly improved its photostability. Previous studies revealed that light degradation mechanism is derived largely from excitation of the flavylium cation (Oliveira et al., 2020), octanoic acid was stacked on the anthocyanidin nucleus through acylation to protect the flavylium cation from excitation (Matsufuji et al., 2007). The C3G and its acylated derivative both followed the first-order degradation kinetics of photo-degradation under either incandescent lamp or UV light (Fig. S2). Furthermore, compared to UV light (456.02), C3G-octanoic acid exhibited longer $t_{1/2}$ under indoor incandescent light condition (563.53). Our findings revealed that C3G acylation with medium chain fatty acid (octanoic acid) enhanced both thermostability and photostability. Establishment of structure activity relationship with other fatty acid moieties of different chain numbers or degree of unsaturation that could aid yield even more stable anthocyanin analogues (Wang et al., 2022) should be further examined.

Table 1
Kinetic parameters for the thermal-degradation and photodegradation of C3G and its derivative. k (h-1), rate constant; t 1/2, half-life time.

Stability	Condition	Sample	k (h-1)	t 1/2
Thermostability	65	C3G	0.10618 (0.9919)	6.5280
		C3G-octaonic acid	0.03875 (0.9815)	17.8877
	80	C3G	0.14926 (0.9841)	4.6439
		C3G-octaonic acid	0.10937 (0.9740)	6.3376
	90	C3G	0.22990 (0.9782)	3.0150
		C3G-octaonic acid	0.13304 (0.9713)	5.1960
Photostability	Incandescent light	C3G	0.00615 (0.9806)	112.71
		C3G-octaonic acid	0.00123 (0.9868)	563.53
	UV	C3G	0.00202 (0.9985)	343.14
		C3G-octaonic acid	0.00152 (0.9953)	456.02

3.3. pH-color response characteristics

The pH-color response process of C3G and its derivative at pH 1.0 till pH 12.0 were shown in Fig. 4. Firstly, the color of C3G and C3G-octanoic acid solution were bright red at low pH (pH 1.0–3.0) (Fig. 4A) attributed to that the flavylium cation (red color) was the predominant species. As the pH value increased (pH 4.0–6.0), the red color of anthocyanin solution gradually faded to pale pink. At this stage, the absorbance of C3G and C3G-octanoic acid decreased with increase in pH (Fig. 4B A_0 and A_1), while the absorbance downtrend of C3G-octanoic acid was slower than C3G, and the peak absorbance of C3G and its derivative red shifted towards longer wavelengths (Fig. 4B B_0 and B_1). Acyl (octanoic acid) protects the flavylium cation from hydration thereby hindering the formation of colorless hemiacetals and to present additional stability to acylated ACNs (Fei et al., 2021). At pH value of 7.0, part of the flavylium cation, hemiacetal and chalcones changed into purple quinonoid bases, which cause the color of C3G and its derivative solution to become purple and to undergo a bathochromic shift (Fig. 4B C_0 and C_1). As the concentration of OH^- increases with pH, anthocyanins mainly exist in quinonoid bases (Neves et al., 2022). Meanwhile, the color of the solution became darker and changed from purple to blue-violet (pH 8.0–9.0), concurrent with an increase in absorbance (Cheng et al., 2022). In the last phase of the pH-color at extreme alkaline pH (pH 11.0–12.0), C3G and its derivative with decrease in absorbance and red shift to 578 nm leading to color change to amber (Fig. 4B D_0 and D_1), due to the quinonoid bases would lose a proton and transform into anionic quinonoid bases (Rawdkuen et al., 2020). At pH 11.0, acylated ACNs exhibit a much higher absorbance at 578 nm compared with natural ACNs mediated via acylation to impart greater stability to the molecule.

It has been shown in Fig. 4 that the two anthocyanins (C3G and acylation C3G) exhibited comparable but slightly different pH-color response characteristics, which can be distinguished visually. Notably, color stability of ACNs based films is crucial when the films are applied to monitor the freshness of food products (Yong et al., 2020). According to these results, acylation with octanoic acid appears as a promising tool to enhance pH color stability of ACNs, and improving pH-sensitive packaging film response based on acylated ACNs compared to natural ACNs (Zhao et al., 2021). In fact, acylated ACNs-rich plants (such as red cabbage, purple sweet potato and black carrot) were better posed as pH-sensitive indicators in intelligent food packaging (Jiang et al., 2020;

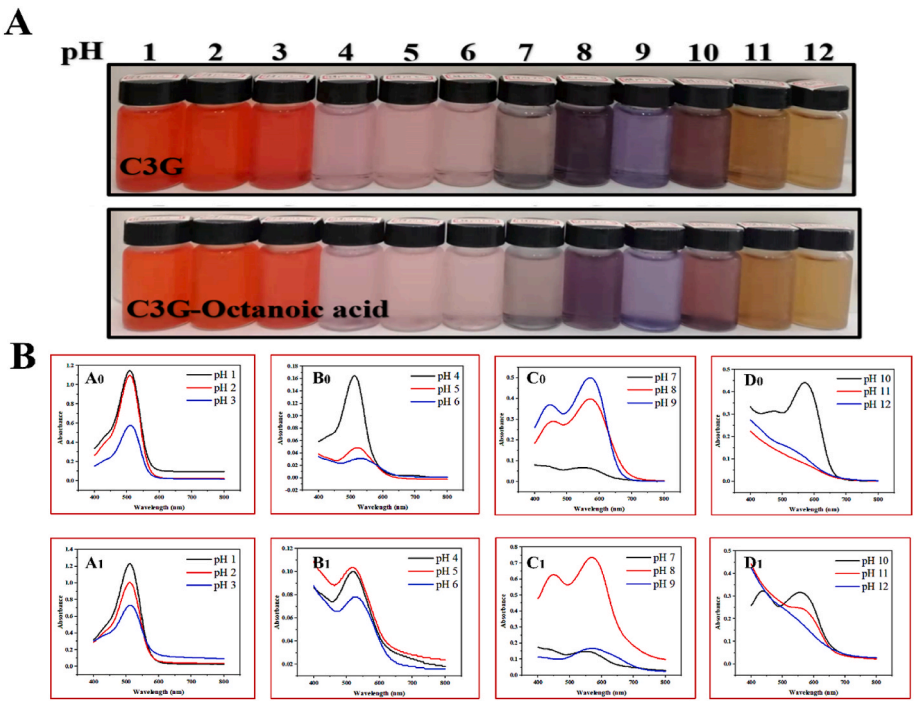

Fig. 4. Color of C3G and its derivative solutions at different pH values (A); UV–vis spectra of the C3G (A0, B0, C0, D0) and its derivative (A1, B1, C1, D1) solutions at different pH values. (For interpretation of the references to color in this figure legend, the reader is referred to the Web version of this article.)

Rawdkuen et al., 2020). Octanoic acid acylated ACNs as a more color stable indicator provides a new source for the development of intelligent packaging.

3.4. NH_3-color response characteristics

During the spoilage of food, for example, meat and aquatic food products, proteins can be degraded by microorganisms to produce various volatile nitrogenous compounds (such as ammonia, dimethylamine and trimethylamine), thereby changing the pH status of food. Therefore, real-time monitoring of changes in food pH throughout the supply chain using pH-sensitive indicators to track the freshness/spoilage of packed food will become more applicable in the future (Oladzadabbasabadi et al., 2022). The basic color change mechanism of anthocyanins could be ascribed to increased levels of volatile amines produced by spoilage microorganisms, which cause increase in pH level concurrent by a color change as observed by the naked eye (Shao et al., 2021). Till now, ACNs-rich films have been used as natural pH indicators to monitor the freshness of protein-rich food products, such as fish, shrimp, chicken, pork, milk and cheese (Kan et al., 2022; You et al., 2022). Previous studies have revealed that the pH-sensitivity of ACNs-rich films can be determined by immersing the films in different buffer solutions or upon exposure to ammonia gases (Kang et al., 2020; Mushtaq et al., 2018). Therefore, response characteristics of acylated C3G to NH_3 was determined in order to provide a theoretical basis for the application of acylated C3G as a pH-sensitive indicator in smart food packaging. In our current research, the principle of C3G and acylated C3G discoloration as colorimetric indicators is depicted in Fig. 5C.

As shown in Fig. 5A, C3G and its derivative solution displayed a dark pink color. The initial absorbance value at 510 nm of C3G solution reached 0.96, and then rapidly decreased to 0.25 and 0.16 at 10 min and 20 min, respectively. Afterwards, absorbance of C3G solution continually declined with maximum absorption peak red-shifted to longer wavelength 524 nm (at 40 min) and 532 nm (at 60 min) at the same time. The dark pink color faded within 60 min with the color of C3G-octanoic acid to fade at a slower rate compared to C3G. Extension of exposure time, maximum absorption peak eventually moved to 584 nm (at 180 min) and the color of C3G and C3G-octanoic acid solution gradually turned to amber. The mechanism of color change lies in that volatized ammonia combines with water in anthocyanin solution to

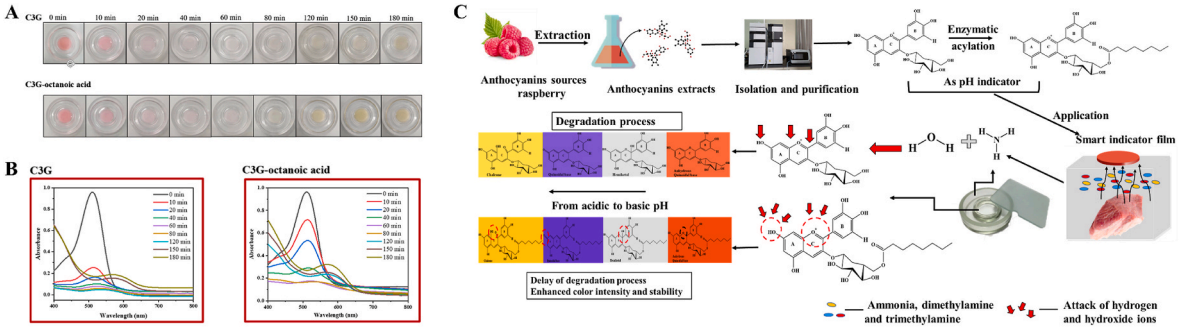

Fig. 5. Color of C3G (A0) and its derivative (A1) solutions in ammonia; UV–Vis spectra of C3G (B0) and its derivatives (B1) in NH3 gas environment; schematic operating mode of C3G and acylated C3G as colorimetric indicators (C). (For interpretation of the references to color in this figure legend, the reader is referred to the Web version of this article.)

form $NH_3{\cdot}H_2O$, and then hydrolyses to form NH_4^+ and OH^- leading to an increase in pH of solution (Yba et al., 2021). Upon solution pH switch from acidic to basic, color of C3G solution changed from red to amber, whereas C3G-octanoic acid solution showed a deeper amber color compared with C3G at alkaline condition. The above results confirmed that NH_3 evaporating off of the ammonia solution were absorbed by anthocyanin solution, with acylated C3G to exert a stronger resistance to pH changes (Liang et al., 2019). Since the molecular chains of octanoic acid intertwined upon the benzene ring of anthocyanins leading to an enhancement of C3G color intensity (Sha et al., 2021). Such higher color intensity of acylated C3G was more distinguishable to discern spoiled products with naked eye than C3G, however, the sensitivity and accuracy may be affected. Therefore, their application in intelligent food packaging remains challenging from such perspective (Fernandez-Aulis et al., 2020) and warranting for future improvements to be applied at a commercial scale.

4. Conclusions

In this study, major ACN (C3G) was firstly isolated from raspberry, further subjected to acylation with octanoic acid at the 6″-OH of the glucose unit in cyanidin to yield a novel acylated derivative. Both thermostability and photostability of C3G were improved post acylation as manifested by lower rate constant (k) and extended $t_{1/2}$ values. Post acylation, C3G-octanoic acid exhibited improved antioxidant capacity. Results of the color response under different pH conditions and NH_3 response indicated that the acylated product has potential applications in intelligent food packaging field. Overall, our results provide novel insights in expanding the application of natural anthocyanins in food industries, meanwhile, also providing a theoretical basis for developing acylated raspberry anthocyanins application in food intelligent packaging. Nevertheless, synthesis of acylated ACNs suffers from low reaction yield warranting for optimization process to furnish efficient synthesis procedure of acylated ACNs.

CRediT authorship contribution statement

Yang Lin: Writing – review & editing, Data curation, Methodology. **Cong Li:** Writing – original draft, Data curation, Investigation, Methodology. **Ping Shao:** Writing – review & editing, Methodology. **Ligang Jiang:** Writing – review & editing. **Bilian Chen:** Investigation, Revising. **Mohamed A. Farag:** Writing – review & editing.

Declaration of competing interest

The authors declare that they have no known competing financial interests or personal relationships that could have appeared to influence the work reported in this paper.

Data availability

Data will be made available on request.

Acknowledgements

This work was supported by National Natural Science Foundation of China (No. 32102006, 32072149), Zhejiang province key research and development program (No. 2019C02070), Quzhou city research and development program (No. 2022K25), Zhejiang Provincial Department of Education Project (No. Y202147379).

Appendix A. Supplementary data

Supplementary data to this article can be found online at https://doi.org/10.1016/j.crfs.2022.11.008.

References

Almasi, H., Forghani, S., Moradi, M., 2022. Recent advances on intelligent food freshness indicators: an update on natural colorants and methods of preparation. Food Packag. Shelf Life 32, 100839.
Araújo, M.D., Franco, Y., Messias, M., Longato, G., Pamphile, J., Carvalho, P., 2017. Biocatalytic synthesis of flavonoid esters by lipases and their biological benefits. Planta Med. 83, 7–22, 01/02.
Bailon, R.M., Gonzalo, C., Santosbuelga, C., 2004. Anthocyanins in cereals. J. Chromatogr. A 1054, 129–141.
Becerril, R., Nerín, C., Silva, F., 2021. Bring some colour to your package: freshness indicators based on anthocyanin extracts. Trends Food Sci. Technol. 111, 495–505.
Cai, J., Zeng, F.S., Zheng, S.Y., Huang, X.X., Zhang, J.Y., Zhang, P., Fei, P., 2020. Preparation of lipid-soluble bilberry anthocyanins through acylation with cinnamic acids and their antioxidation activities. J. Agric. Food Chem. 68 (28), 7467–7473.
Cai, D., Li, X., Chen, J., et al., 2022. A comprehensive review on innovative and advanced stabilization approaches of anthocyanin by modifying structure and controlling environmental factors[J]. Food Chem. 366, 130611.
Cheng, M., Yan, X., Cui, Y., Han, M., Wang, X., Wang, J., Zhang, R., 2022. An eco-friendly film of pH-responsive indicators for smart packaging. J. Food Eng. 321, 110943.
Cruz, L., Benohoud, M., Rayner, C.M., Mateus, N., De Freitas, V., Blackburn, R.S., 2018. Selective enzymatic lipophilization of anthocyanin glucosides from blackcurrant (*Ribes nigrum* L.) skin extract and characterization of esterified anthocyanins. Food Chem. 266 (15), 415–419.
Cruz, L., Fernandes, I., Guimaraes, M., de Freitas, V., Mateus, N., 2016. Enzymatic synthesis, structural characterization and antioxidant capacity assessment of a new lipophilic malvidin-3-glucoside-oleic acid conjugate. Food Funct. 7 (6), 2754–2762.
Cruz, L., Guimaraes, M., Araujo, P., Evora, A., de Freitas, V., Mateus, N., 2017. Malvidin 3-glucoside-fatty acid conjugates: from hydrophilic toward novel lipophilic derivatives. J. Agric. Food Chem. 65 (31), 6513–6518.
Dangles, O., Saito, N., Brouillard, R., 1993. Anthocyanin intramolecular copigment effect. Phytochemistry 34 (1), 119–124.
Fei, P., Zeng, F., Zheng, S., Chen, Q., Hu, Y., Cai, J., 2021. Acylation of blueberry anthocyanins with maleic acid: improvement of the stability and its application potential in intelligent color indicator packing materials. Dyes Pigments 184, 108852.
Fernandez-Aulis, F., Torres, A., Sanchez-Mendoza, E., Cruz, L., Navarro-Ocana, A., 2020. New acylated cyanidin glycosides extracted from underutilized potential sources: enzymatic synthesis, antioxidant activity and thermostability. Food Chem. 309, 125796.
Filho, J., Braga, A., Oliveira, B., Gomes, F.P., Egea, M.B., 2021. The potential of anthocyanins in smart, active, and bioactive eco-friendly polymer-based films: a review. Food Res. Int. 142 (30), 110202.
Ge, Y., Li, Y., Bai, Y., Yuan, C., Wu, C., Hu, Y., 2020. Intelligent gelatin/oxidized chitin nanocrystals nanocomposite films containing black rice bran anthocyanins for fish freshness monitorings. Int. J. Biol. Macromol. 155, 1296–1306.
Grajeda-Iglesias, C., Salas, E., Barouh, N., Barea, B., Figueroa-Espinoza, M.C., 2017. Lipophilization and MS characterization of the main anthocyanins purified from hibiscus flowers. Food Chem. 230, 189–194.
Jiang, G., Hou, X., Zeng, X., Zhang, C., Wu, H., Shen, G., Zhang, Z., 2020. Preparation and characterization of indicator films from carboxymethyl-cellulose/starch and purple sweet potato (*Ipomoea batatas* (L.) lam) anthocyanins for monitoring fish freshness. Int. J. Biol. Macromol. 143, 359–372.
Kang, S., Wang, H., Xia, L., Chen, M., Li, L., Cheng, J., Jiang, S., 2020. Colorimetric film based on polyvinyl alcohol/okra mucilage polysaccharide incorporated with rose anthocyanins for shrimp freshness monitoring. Carbohydr. Polym. 229, 115402.
Kan, J., Liu, J., Xu, F., Yun, D., Yong, H., Liu, J., 2022. Development of pork and shrimp freshness monitoring labels based on starch/polyvinyl alcohol matrices and anthocyanins from 14 plants: a comparative study. Food Hydrocolloids 124, 107293.
Kurek, M., Garofulić, I.E., Bakić, M.T., Ščetar, M., Uzelac, V.D., Galić, K., 2018. Development and evaluation of a novel antioxidant and pH indicator film based on chitosan and food waste sources of antioxidants. Food Hydrocolloids 84, 238–246.
Liang, T., Sun, G., Cao, L., Li, J., Wang, L., 2019. A pH and NH3 sensing intelligent film based on *Artemisia sphaerocephala Krasch.* gum and red cabbage anthocyanins anchored by carboxymethyl cellulose sodium added as a host complex. Food Hydrocolloids 87, 858–868.
Li, L., Zhou, P., Wang, Y., Pan, Y., Chen, M., Tian, Y., Zheng, J., 2022. Antimicrobial activity of cyanidin-3-O-glucoside-lauric acid ester against *staphylococcus aureus* and *escherichia coli*. Food Chem. 383, 132410.
Lin, Y., Pangloli, P., Meng, X., Dia, V.P., 2020. Effect of heating on the digestibility of isolated hempseed (*Cannabis sativa* L.) protein and bioactivity of its pepsin-pancreatin digests. Food Chem. 314, 126198.
Liu, J., Zhuang, Y., Hu, Y., Xue, S., Li, H., Chen, L., Fei, P., 2020. Improving the color stability and antioxidation activity of blueberry anthocyanins by enzymatic acylation with p-coumaric acid and caffeic acid. LWT- Food Science and Technology. 130, 109673.
Matsufuji, H., Kido, H., Misawa, H., Yaguchi, J., Otsuki, T., Chino, M., et al., 2007. Stability to light, heat, and hydrogen peroxide at different pH values and DPPH radical scavenging activity of acylated anthocyanins from red radish extract. J. Agric. Food Chem. 55 (9), 3692–3701.
Meng, L.S., Guang, Xin, Bin, Li, Dongnan, Tingcai, 2018. Anthocyanins extracted from *Aronia Melanocarpa* protect SH-SY5Y cells against amyloid-beta (1-42)-induced apoptosis by regulating Ca^{2+} homeostasis and inhibiting mitochondrial dysfunction. J. Agric. Food Chem. 66 (49), 12967–12977.

Mushtaq, M., Gani, A., Gani, A., Punoo, H.A., Masoodi, F.A., 2018. Use of pomegranate peel extract incorporated zein film with improved properties for prolonged shelf life of fresh Himalayan cheese (Kalari/kradi). Innovat. Food Sci. Emerg. Technol. 48, 25–32.
Neves, D., Andrade, P.B., Videira, R.A., de Freitas, V., Cruz, L., 2022. Berry anthocyanin-based films in smart food packaging: a mini-review. Food Hydrocolloids 133, 107885.
Oladzadabbasabadi, N., Mohammadi Nafchi, A., Ghasemlou, M., Ariffin, F., Singh, Z., Al-Hassan, A.A., 2022. Natural anthocyanins: sources, extraction, characterization, and suitability for smart packaging. Food Packag. Shelf Life 33, 100872.
Oliveira, H., Correia, P., Pereira, A.R., Araujo, P., Mateus, N., de Freitas, V., 2020. Exploring the applications of the photoprotective properties of anthocyanins in biological systems. Int. J. Mol. Sci. 21 (20), 7464.
Plaza, M., Pozzo, T., Liu, J., Gulshan Ara, K.Z., Turner, C., Nordberg Karlsson, E., 2014. Substituent effects on in vitro antioxidizing properties, stability, and solubility in flavonoids. J. Agric. Food Chem. 62 (15), 3321–3333.
Qin, Y., Yun, D., Xu, F., Chen, D., Kan, J., Liu, J., 2021. Smart packaging films based on starch/polyvinyl alcohol and lycium ruthenicum anthocyanins-loaded nano-complexes: functionality, stability and application. Food Hydrocolloids 119, 106850.
Rawdkuen, S., Faseha, A., Benjakul, S., Kaewprachu, P., 2020. Application of anthocyanin as a color indicator in gelatin films. Food Biosci. 36, 100603.
Scano, P., 2021. Characterization of the medium infrared spectra of polyphenols of red and white wines by integrating FT IR and UV-Vis spectral data. LWT- Food Science and Technology. 147 (1), 111604.
Sha, B., Gw, B., Hl, B., Yx, B., Xl, B., Hl, B., 2021. Preparation and dynamic response properties of colorimetric indicator films containing pH-sensitive anthocyanins. Sens. Actuator. Rep. 3, 100049.
Shao, P., Liu, L., Yu, J., Lin, Y., Gao, H., Chen, H., Sun, P., 2021. An overview of intelligent freshness indicator packaging for food quality and safety monitoring. Trends Food Sci. Technol. 118, 285–296.
Song, Z., Na, M.A., Yue, L., Sc, A., Yx, A., 2021. Antioxidant activities of lipophilic (-)-epigallocatechin gallate derivatives in vitro and in lipid-based food systems. Food Biosci. 42, 101055.
Sreerekha, P.R., Dara, P.K., Vijayan, D.K., Chatterjee, N.S., Raghavankutty, M., Mathew, S., Anandan, R., 2021. Dietary supplementation of encapsulated anthocyanin loaded-chitosan nanoparticles attenuates hyperlipidemic aberrations in male wistar rats. Carbohydrate Poly. Technol. Appl. 2, 100051.
Taghavi, T., Patel, H., Akande, O.E., Galam, D.C.A., 2022. Total anthocyanin content of strawberry and the profile changes by extraction methods and sample processing. Foods 11, 1072.
Tarone, A.G., Cazarin, C.B.B., Marostica Junior, M.R., 2020. Anthocyanins: new techniques and challenges in microencapsulation. Food Res. Int. 133, 109092.
Teng, H., Mi, Y., Cao, H., Chen, L., 2021. Enzymatic acylation of raspberry anthocyanin: evaluations on its stability and oxidative stress prevention. Food Chem. 372, 130766.
Wang, P.K., Liu, J.N., Zhuang, Y.H., Fei, P., 2022. Acylating blueberry anthocyanins with fatty acids: improvement of their lipid solubility and antioxidant activities. Food Chem. X 15, 100420.
Xiao, D., Jin, X., Song, Y., Zhang, Y., Li, X., Wang, F., 2021. Enzymatic acylation of proanthocyanidin dimers from Acacia mearnsii bark: effect on lipophilic and antioxidant properties. J. Bioresour. Bioprod. 6 (4), 359–366.
Yan, Z., Li, C., Zhang, L., Liu, Q., Ou, S., Zeng, X., 2016. Enzymatic acylation of anthocyanin isolated from black rice with methyl aromatic acid ester as donor: stability of the acylated derivatives. J. Agric. Food Chem. 64 (5), 1137–1143.
Yang, W., Kortesniemi, M., Ma, X., Zheng, J., Yang, B., 2019. Enzymatic acylation of blackcurrant (*Ribes nigrum*) anthocyanins and evaluation of lipophilic properties and antioxidant capacity of derivatives. Food Chem. 281, 189–196.
Yang, W., Kortesniemi, M., Yang, B., Zheng, J., 2018. Enzymatic acylation of anthocyanins isolated from *Alpine Bearberry (Arctostaphylos Alpina)* and lipophilic properties, thermostability, and antioxidant capacity of the derivatives. J. Agric. Food Chem. 66 (11), 2909–2916.
Yba, B., Hca, B., Jta, B., Yda, B., Qta, B., Wza, B., Dla, B., 2021. Novel pH sensitivity and colorimetry-enhanced anthocyanin indicator films by chondroitin sulfate co-pigmentation for shrimp freshness monitoring. Food Control 131, 108441.
Yong, H., Liu, J., 2020. Recent advances in the preparation, physical and functional properties, and applications of anthocyanins-based active and intelligent packaging films. Food Packag. Shelf Life 26, 100550.
You, S., Zhang, X., Wang, Y., Jin, Y., Wei, M., Wang, X., 2022. Development of highly stable color indicator films based on kappa-carrageenan, silver nanoparticle and red grape skin anthocyanin for marine fish freshness assessment. Int. J. Biol. Macromol. 216, 655–669.
Zhang, P.L., Liu, S., Zhao, Z.G., You, L.J., Harrison, M.D., Zhang, Z.Y., 2021. Enzymatic acylation of cyanidin-3-glucoside with fatty acid methyl esters improves stability and antioxidant activity. Food Chem. 343, 128482.
Zhao, C.L., Yu, Y.Q., Chen, Z.J., Wen, G.S., Wei, F.G., Zheng, Q., Xiao, X.L., 2017. Stability-increasing effects of anthocyanin glycosyl acylation. Food Chem. 214, 119–128.
Zhao, L., Pan, F., Mehmood, A., Zhang, H., Ur Rehman, A., Li, J., Wang, C., 2021. Improved color stability of anthocyanins in the presence of ascorbic acid with the combination of rosmarinic acid and xanthan gum. Food Chem. 351, 129317.